The accretion disk evolution and the Spectral Energy Distribution (SED)

Stellar Formation and Circumstellar Medium - Practical Work

Telmo Monteiro[1]

Department of Physics and Astronomy, University of Porto, Rua do Campo Alegre 1021 1055, 4169-007 Porto
e-mail: up202308183@up.pt

April 7, 2024

ABSTRACT

Aims. Explore the evolution of a viscous accretion disk, analysing its dependencies on parameters such as viscosity, and estimate the total Spectral Emission Distribution (SED), $\lambda F\lambda$, of a stellar system with a circumstellar disk.
Methods. For the first part, we used the analytical solution for the diffusion equation and the forward-Euler method for numerical approaches. In the second part, we modelled the SED of each component by making use of approximations like black-body radiation and the Simpson's rule for integration approximations.
Results. We were able to study the evolution of the surface mass density as a function of radius, time and viscosity and to model the joint and separate SED of four components, changing parameters such as mass accretion rate, effective temperature and stellar mass.

Key words. accretion disk evolution – stellar formation – Spectral Energy Distribution

1. Introduction

Young protostars primarily amass mass through gas accretion from the circumstellar disks encircling them, establishing a direct link between star formation and disk evolution. For this reason, the formation of planetary systems naturally arises in the later stages of protostellar disk evolution.

This project aims to study these disks. As in many cases, the disk flow is confined so closely to the orbital plane that to a first approximation one can regard the disc as a two-dimensional gas flow. This thin disc approximation has proved very successful, allowing an elaborate theory to be developed. The exploration of protoplanetary disks encircling young stars is still a growing field of research, which interest stems from the encouraging results of comparison between theory and observations of close binary systems (Frank, J., King, A., & Raine, D. (2002)).

Initially, our focus lies on analytically solving the diffusion equation over time for a constant viscosity, ν_0, originated from an initial thin annulus of material at a distance r_0 from the star. We examine how the diffusion evolution time scale alters with increasing viscosity, comparing the numerical and analytical results. Furthermore, we scrutinize the outcomes by manipulating parameters such as the exponential parameter β, viscosity ν, and initial distance between the star and the annulus r_0.

The second part of this project was to study the Spectral Energy Distribution (SED) of a star with a steady thin and optically thick disk, analysing the emission of four components (stellar radiation, disk emission due to viscosity and due to stellar irradiation and boundary layer emission). Observationally, it is quite difficult to separate each component from the other, but to further study this systems one has to model their separate and joint SED, changing parameters such as effective temperature, stellar mass and mass accretion rate.

2. The accretion disk evolution

The evolution of a viscous accretion disk depends upon the behaviour of the viscosity, which in turn can depend in an unknown way on the disk properties. However it is possible to explore some simple solutions of the diffusion equation

$$\frac{\partial \Sigma}{\partial t} = \frac{3}{r}\frac{\partial}{\partial r}\left[r^{1/2}\frac{\partial}{\partial r}(\nu\Sigma r^{1/2})\right], \tag{1}$$

which show some general properties of accretion disks (Frank, J., King, A., & Raine, D. (2002), Gameiro, J.F.S. (2024)).

We want to study the analytical and numerical approaches to solve this diffusion equation. For this, we consider an initial thin annulus of material at a distance r_0 to the star, starting with an initial density distribution representing the annulus of matter

$$\Sigma(r, t = 0) = \frac{M_d}{2\pi r_0}\delta(r - r_0). \tag{2}$$

2.1. Analytical solution of the diffusion equation

Lynden-Bell, D. & Pringle, J.E. (1974) showed that for a constant viscosity ν_0 the solution is given by

$$\Sigma(x, \tau) = \frac{M_d}{\pi r_0^2}x^{-1/4}\tau^{-1}\exp\left[-\frac{(1 + x^2)}{\tau}\right]I_{1/4}\left(\frac{2x}{\tau}\right), \tag{3}$$

where $I_{1/4}$ is the modified Bessel function of fractional order, $x = r/r_0$ is the dimensionless distance and $\tau = 12\nu t/r_0^2$ a dimensionless time. As initial conditions, we took the mass of the disk as $M_d = 0.01M_\odot$, $\nu_0 = 10^{17}$ cm^2 s^{-1}, $R_\star = 2R_\odot$, $M_\star = 1M_\odot$, the inner part of the disk $r_{\rm in} = R_\star$, the outer part of the disk $r_{\rm out} = 200R_\star$ and $r_0 = r_{\rm out}/2$. We also considered $M_\odot = 1.99 \times 10^{33}$ g, $R_\odot = 6.96 \times 10^{10}$ cm.

Figure 1a consists in a replica of figure 5.1 from Frank, J., King, A., & Raine, D. (2002), being the plotted dimensionless times τ very similar. Figure 1b zooms on the region near the outer border of the disk. From these two figures, one can see that the initial ring of material spreads and as the time proceeds there is a concentration of mass at smaller radii, being pulled into the star neighborhood, and the total mass is decreasing as a part of it is accreted onto the star. At the same time, some mass is pushed to large distance to conserve angular momentum.

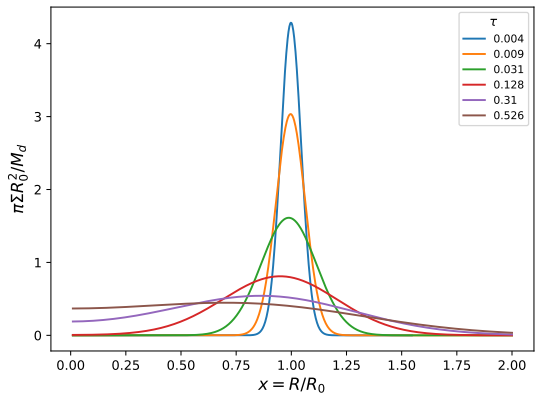

(a) Total disk.

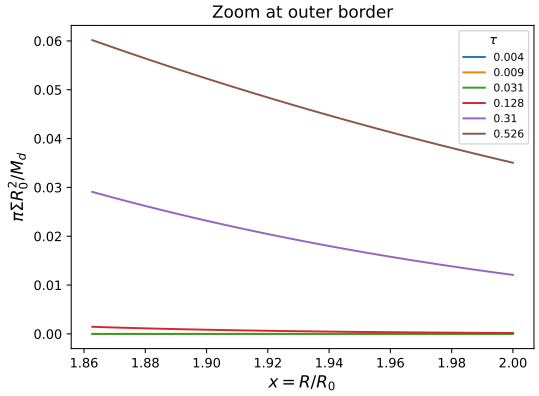

(b) Zoom at the outer border region of the disk.

Fig. 1: Ring of matter of mass M_d placed in a Kepler orbit at $R = R_0$ spreading out using the analytical approach. The surface density Σ, given by equation 3, is shown as a function of $x = R/R_0$, the normalized distance, in the dimensionless form by multiplying it by a factor of $\pi R_0^2/M_d$.

For a different visualization, the reader can refer to figure A.1 in the appendix, which shows a 2-D plot of τ as a function of x, forming a plume-esque evolution of the surface mass density.

The next step was to analyse how the diffusion evolution time scale changes with increasing the viscosity. For that, we compared the surface mass density in function of x plot for three values of viscosity: ν_0, $10\nu_0$ and $100\nu_0$, as shown in figure 2. As one can see, the dimensionless time τ increases with viscosity and the surface mass density decreases overall in the disk. This last aspect can be seen in figure 4, where the integrated (total) surface mass density decreases inversely proportional to viscosity, while the last τ increases. Additionally, opposite to what happens when $\nu = \nu_0$, in the cases $\nu = 10\nu_0$ and $\nu = 100\nu_0$ the mass only tends to accumulate in the outer border of the disk for part of the evolution time scale, changing half way to decrease in this part of the disk. This is better depicted in figure 3, while in the original system the dimensionless surface mass density in the border increases in a linear fashion, in the other two cases it decreases faster with increasing viscosity.

2.2. Numerical solution of the diffusion equation

We integrated numerically the diffusion equation, starting with the initial density distribution as in equation 2. For this, we used the finite differences approach to the forward-Euler method, as described in Langtangen, H.P., & Linge, S. (2017). We consider the time variable for the evolution $t = n\Delta t$, with $n = 0, 1, ..., N_t$, and the distance variable in the disk plane (distance to the star) $r = j\Delta r$, with $j = 0, 1, ..., N_r$, and write $\Sigma(r, t) = \Sigma_r^t = f_j^n$. This way, one can write derivatives in order to r and t as

$$\begin{cases} \frac{\partial f_j^n}{\partial t} = \frac{f_j^{n+1} - f_j^n}{\Delta t} \\ \frac{\partial f_j^n}{\partial r} = \frac{f_{j+1}^n - f_j^n}{\Delta r} \\ \frac{\partial^2 f_j^n}{\partial r^2} = \frac{f_{j+1}^n - 2f_j^n + f_{j-1}^n}{\Delta r} \end{cases} \tag{4}$$

So, if one considers constant ν, equation 1 becomes

$$\frac{\partial \Sigma}{\partial t} = \frac{3\nu}{r}\left[\frac{3}{2}\frac{\partial \Sigma}{\partial r} + r\frac{\partial^2 \Sigma}{\partial r^2}\right]. \tag{5}$$

Inserting the equations of the system 4 and using $r = j\Delta r$,

$$f_j^{n+1} = f_j^n + \frac{3\nu}{j\Delta r^2}\left[\frac{3}{2}\left(f_{j+1}^n - f_j^n\right) + j\left(f_{j+1}^n - 2f_j^n + f_{j-1}^n\right)\right]. \tag{6}$$

To assure that this equation converges and a solution is obtained, we consider the stability criterion $2D\Delta t/\Delta r^2$, where $D = 3\nu_0$. In the case $\nu = \nu_0$, the stability criterion is 0.30965. We considered the boundary conditions $\Sigma(R_\star, t) = 0$ and $\Sigma(R_{\rm out}, t) = 0$. This said, we were able to obtain figure 5. Although figure 5 is very similar to figure 1a, two striking differences can be noted: first, that the surface mass density near the outer edge of the disk falls to zero in every given time (a byproduct of the boundary condition), and, second, that the order of magnitude of the surface mass density axis is several times bigger than in figure 1a. The reason for this last difference is not yet comprehended.

A two-dimensional plot in the same fashion of figure A.1 can be seen in figure A.2 in the appendix. For better visualization the color map was scaled using Z-scaling. It's also evident the movement of mass towards the center of the disk as time passes.

Next we studied the case where viscosity takes a dependence with distance to the star, $\nu = \nu_0\left(\frac{r}{r_0}\right)^\beta$. In this case, we can rewrite equation 1 by expanding the derivatives in

$$\frac{\partial \Sigma}{\partial t} = \frac{3}{r}\left[\frac{3}{2}\Sigma\frac{\partial \nu}{\partial r} + \frac{3}{2}\nu\frac{\partial \Sigma}{\partial r} + 2r\frac{\partial \nu}{\partial r}\frac{\partial \Sigma}{\partial r} + r\Sigma\frac{\partial^2 \nu}{\partial r^2} + r\nu\frac{\partial^2 \Sigma}{\partial r^2}\right]. \tag{7}$$

We also compute the derivatives of $\nu = \nu_0\left(\frac{r}{r_0}\right)^\beta$:

$$\begin{cases} \frac{\partial \nu}{\partial r} = \frac{\beta}{r}\left(\frac{r}{r_0}\right)^\beta \\ \frac{\partial^2 \nu}{\partial r^2} = \frac{\beta(\beta-1)}{r^2}\nu_0\left(\frac{r}{r_0}\right)^\beta \end{cases} \tag{8}$$

Recalling the system of equations 4 and imputing the derivatives of ν, we obtain the "train" equation to be used in the numerical modelling

$$f_j^{n+1} = f_j^n + \Delta t\frac{3}{r_j}\nu_0\left(\frac{r_j}{r_0}\right)^\beta\left[\frac{3}{2}f_j^n\frac{\beta}{r_j} + \frac{3}{2}\frac{f_{j+1}^n - f_j^n}{\Delta r} + \right.$$
$$\left. + 2r\frac{f_{j+1}^n - f_j^n}{\Delta r}\frac{\beta}{r_j} + 3f_j^n\frac{\beta(\beta-1)}{r_j^2} + 3\frac{f_{j+1}^n - 2f_j^n + f_{j-1}^n}{\Delta r}\right] \tag{9}$$

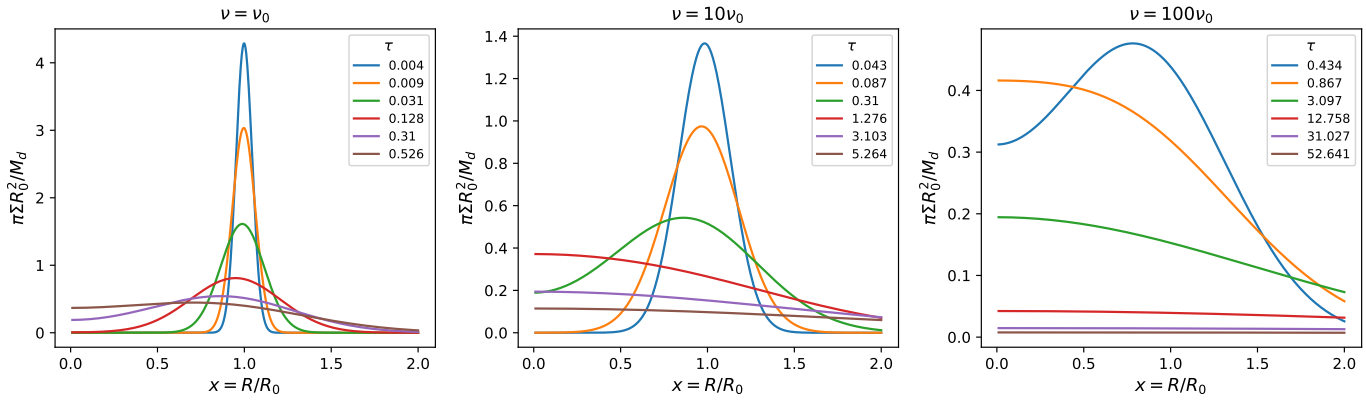

Fig. 2: Ring of matter of mass M_d placed in a Kepler orbit at $R = R_0$ spreading out using the analytical approach. Each plot shows the surface density Σ, in the dimensionless form, as a function of $x = R/R_0$ for viscosity ν set to ν_0, $10\nu_0$ and $100\nu_0$ (from left to right).

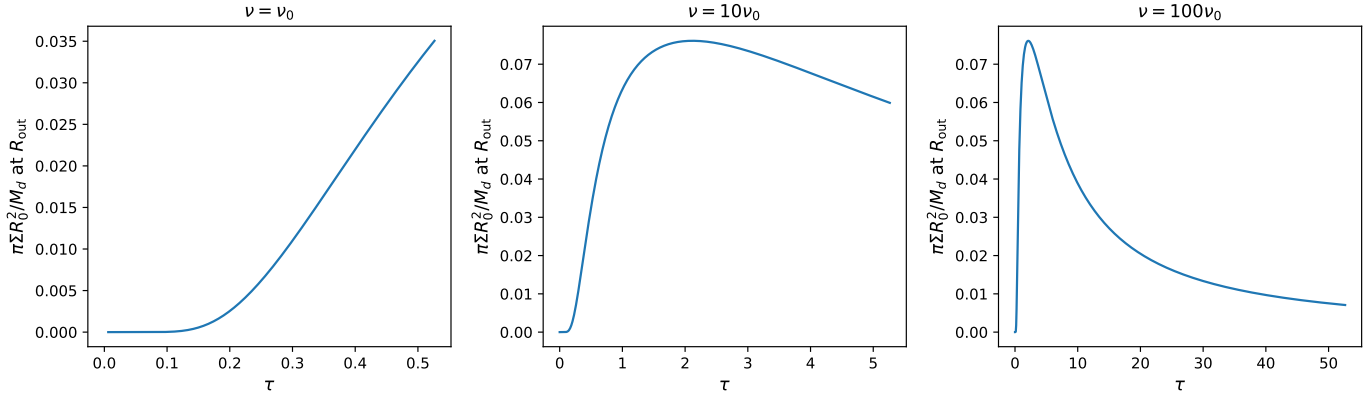

Fig. 3: Dimensionless surface mass density $\pi\Sigma R_0^2/M_d$ in the border of the disk (last point) in function of dimensionless time τ for viscosities ν_0, $10\nu_0$ and $100\nu_0$.

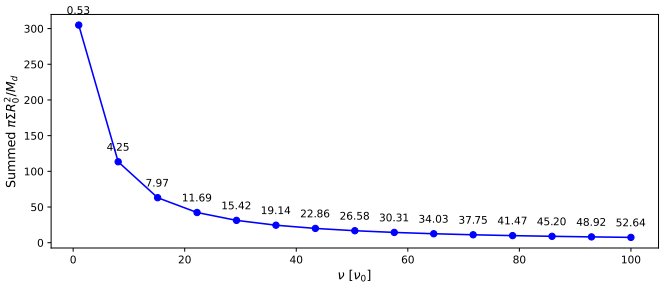

Fig. 4: Summed Dimensionless surface mass density $\pi\Sigma R_0^2/M_d$ summed along the totality of the disk in function of viscosity ν, ranging from nu_0 to $100\nu_0$. The text annotations represent the maximum dimensionless time τ.

We used $\Delta r = 2R_\star$ and $\Delta t = 10^3$ to try to obtain the maximum potential of this modelling, obtaining a stability criterion of 0.00774. We started by changing the parameter β, taking values $\beta \in [-2, -1, 0, 1, 2]$, being the case where $\beta = 0$ the same as seen in figure 5. These values were chosen based on the capabilities of the algorithm to converge, which is not possible for β lower than -2. Figure 6 shows the outcome, where the coloring is related to the same normalized times τ as seen in figure 5. One can observe that when the viscosity increases with radius ($\beta > 0$) the mass tends to accumulate more near the center of the disk in a kind of bulk motion, instead of distributing evenly with radius. The opposite is observed when the viscosity decreases with radius ($\beta < 0$): the mass tends to, slowly, accumulate in radii near the outer border of the disk. For a better view of the effect of β, figure 7 shows the case where $\beta = 7$, the maximum positive value where the algorithm converges.

Figure 8 shows the case where we change the initial position of the material ring, r_0, to either 1/10 or 9/10 of the position of the edge of the disk, r_{out}. In the second case, the material has a tendency to accumulate closer and closer to the center of the disk, opposite to the first case, where the material is already close to the center of the disk.

3. Spectral Energy Distribution (SED) of a star with a circumstellar disk

In this section, we want to analyse a steady thin disk, optically thick, with a density distribution as found in section 2 and with the system presenting the characteristics $M_\star = 1M_\odot$, $R_\star = 2R_\odot$, $T_{\text{eff}} = 4500$ K, $d_\star = 140$ parsec, inclination $i = 60°$ and $V \sin i = 10$ km/s. For the effects of this work, we converted these quantities to SI units.

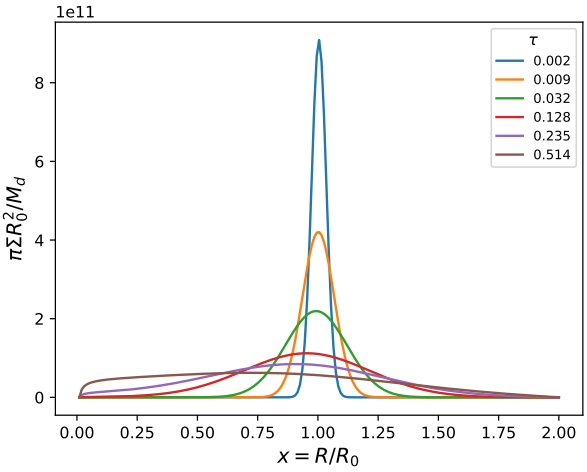

Fig. 5: Ring of matter of mass M_d placed in a Kepler orbit at $R = R_0$ spreading out using the numerical approach. The surface density Σ, given by equation 6, is shown as a function of $x = R/R_0$, the normalized distance, in the dimensionless form by multiplying it by a factor of $\pi R_0^2/M_d$.

We want to estimate the total Spectral Emission Distribution (SED), λF_λ, of the system and the emission from each component for a mass accretion rate $\dot{M} = 10^{-7} M_\odot$ yr^{-1}. The components we need to consider are the stellar emission (assuming black-body emission), the disk emission due to the viscosity, the disk emission caused by stellar irradiation and the boundary layer emission, caused by the star-disk interaction.

3.1. Stellar black-body emission

Assuming the stellar radiation behaves as a black-body emission at temperature $T_{\rm eff}$, the flux at a given wavelength λ is

$$F_\star^\lambda = \pi B_\lambda(T_{\rm eff}), \tag{10}$$

where the Planck function $B_\lambda(T_{\rm eff})$ is given by

$$B_\lambda(T_{\rm eff}) = \frac{2hc^2}{\lambda^5}\left(e^{\frac{hc}{\lambda k_B T_{\rm eff}}} - 1\right)^{-1}. \tag{11}$$

The observed flux at a wavelength λ is obtained using the stellar radius and the distance of the observer to the disk

$$F_{\rm obs}^\lambda = F_\star^\lambda \left(\frac{R_\star}{d}\right)^2. \tag{12}$$

3.2. Disk emission due to the viscosity

$$F_\lambda = \frac{2\pi\cos(i)}{d^2}\int_{r_{in}}^{r_{out}} B_\lambda(T_d(r))r dr, \tag{13}$$

where

$$T_d(r) = \left[\frac{3GM_\star\dot{M}}{8\pi r^3\sigma}\left[1 - \left(\frac{R_\star}{r}\right)^{1/2}\right]\right]^{1/4}. \tag{14}$$

The integral in equation 13 was computed using the Simpson's rule.

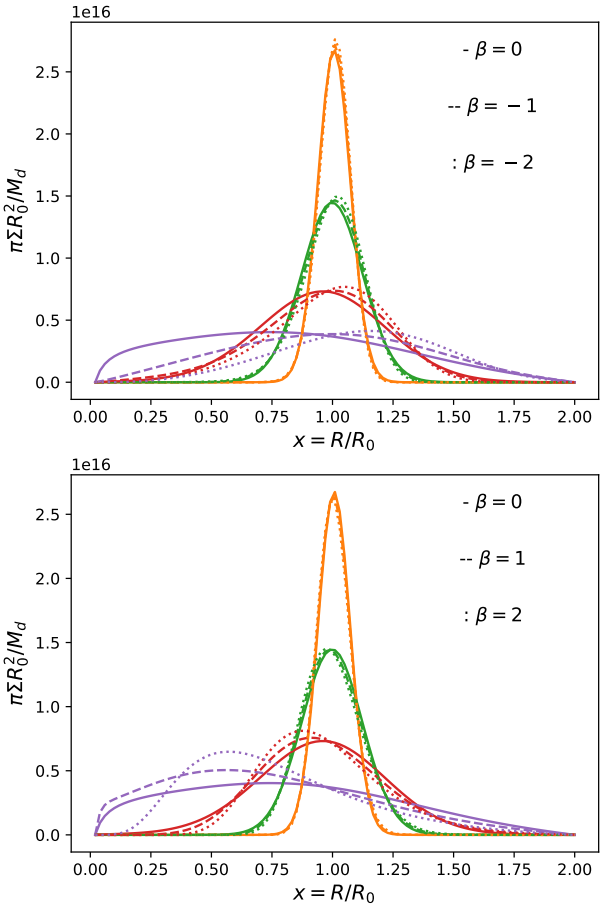

Fig. 6: Ring of matter of mass M_d placed in a Kepler orbit at $R = R_0$ spreading out using the numerical approach for values of β ranging between -2 and 2. For better visualization each plot shows the positive or negative β (and the original case, $\beta = 0$). The surface density Σ is shown as a function of $x = R/R_0$ in the dimensionless form. The first τ shown in blue in the previous figures is omitted for better visualization.

3.3. Disk emission caused by stellar irradiation

The irradiation from the star at a distance r is given by

$$F_{\rm irr}^\lambda(r) = B_\lambda(T_{\rm eff})\left[\arcsin(\frac{R_\star}{r}) - \frac{R_\star}{r}\left[1 - (\frac{R_\star}{r})^2\right]^{1/2}\right]. \tag{15}$$

The total flux that heats the disk at a distance r is

$$F_{\rm irr}(r) = \int F_{\rm irr}^\lambda(r)d\lambda = \sigma T_{\rm irr}^4(r). \tag{16}$$

Then the flux emitted by the disk caused by stellar irradiation is given by

$$F_\lambda = \frac{2\pi\cos(i)}{d^2}\int_{r_{in}}^{r_{out}} B_\lambda(T_{\rm irr}(r))r dr. \tag{17}$$

The integral in equation was computed in a simple way by summing the elements in the $F_{\rm irr}^\lambda(r)$ array and multiplying by $d\lambda$ (dif-

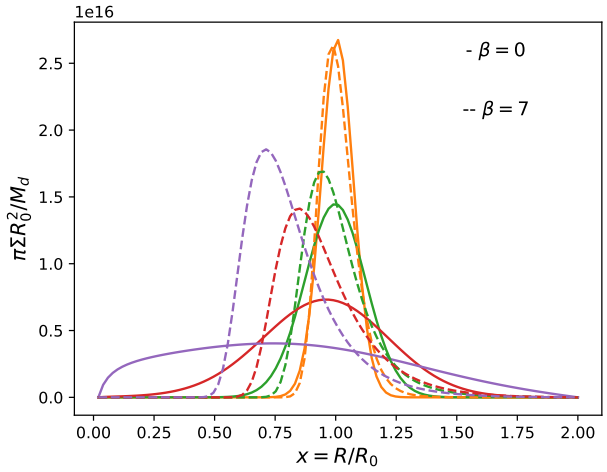

Fig. 7: Ring of matter of mass M_d placed in a Kepler orbit at $R = R_0$ spreading out using the numerical approach $\beta = 0$ and $\beta = 7$, the highest β achieved. The surface density Σ is shown as a function of $x = R/R_0$ in the dimensionless form. The first τ shown in blue in the previous figures is omitted for better visualization.

ference between two consecutive elements in the wavelength array). In the other hand, the integral in equation was computed using Simpson's rule.

3.4. Boundary layer emission

The temperature in the boundary layer is determined by

$$T_{\rm BL}^4 = T_{\rm in}^4 \frac{R_\star}{3H}, \tag{18}$$

where

$$T_{\rm in} = \left(\frac{3GM_\star \dot{M}}{8\pi\sigma R_\star^3}\right)^{1/4}. \tag{19}$$

The thickness of the disk near the surface of the star is given by

$$H^2 = \frac{R_\star^3}{GM_\star} c_s^2, \tag{20}$$

where c_s is the sound speed. We can take the sound speed in the boundary layer similar to the value in the inner part of the disk $c_s^2 \sim \frac{kT_{\rm in}}{\mu m_H}$. We can also assume the matter is completely ionized in the inner part of the disk, $\mu \sim 0.615$, so

$$T_{\rm BL} = T_{\rm in}\left(\frac{GM_\star \mu m_H}{9R_\star kT_{\rm in}}\right)^{1/8}. \tag{21}$$

We know that

$$F_{\rm obs}^\nu = \frac{\pi R_\star^2 \cos(i)}{d^2} B_\nu(T_{\rm BL}) \tag{22}$$

and that

$$L_{\rm BL} = 2 \times 2\pi R_\star H \sigma T_{\rm BL}^4 = \frac{\dot{M}M_\star G}{2R_\star}\left[1 - \frac{\Omega_\star}{\Omega_k}\right]^2. \tag{23}$$

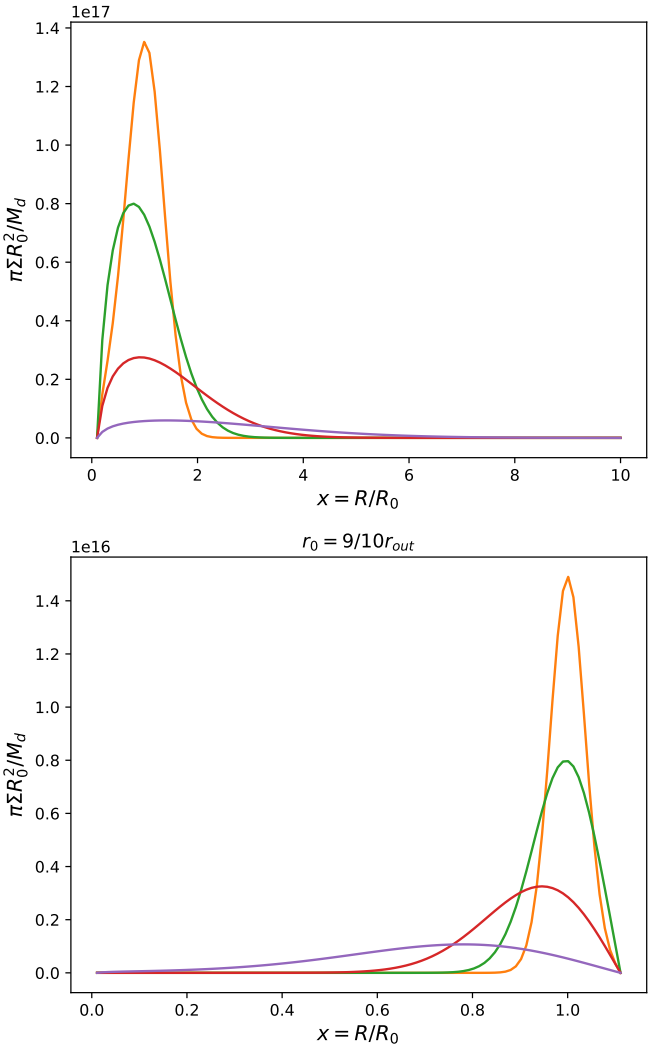

Fig. 8: Ring of mass M_d which is initially positioned at two different positions $R_0 = R_{\rm out}/10$ or $R_0 = \frac{9}{10}R_{\rm out}$. The surface density Σ is shown as a function of $x = R/R_0$ in the dimensionless form. The first τ shown in blue in the previous figures is omitted for better visualization.

$L_{\rm BL}$ varies with occultation of the boundary layer by the star, by $L_{\rm BL}/2 \times f$, with $f < 1$, but we choose to neglect the occultation, so $f \sim 1$. If $T_{\rm BL}$ and H are known, we finally obtain the boundary layer emission

$$F_{\rm obs}^\nu = \frac{2\pi\cos(i)}{d^2}\int_{R_\star}^{R_\star+H} B_\nu(T_{\rm BL}) r dr \tag{24}$$

$$= \frac{2\pi R_\star H}{d^2} B_\nu(T_{\rm BL})\cos(i). \tag{25}$$

3.5. Total flux emission

Figure 9 shows each component of the total flux, as well as the summed flux observed from Earth, consisting in total Spectral Emission Distribution (SED). The total SED resembles a black-body emission distribution, where the component that contributes the most for lower wavelength is the stellar emission and for higher wavelength is the disk emission due to viscosity.

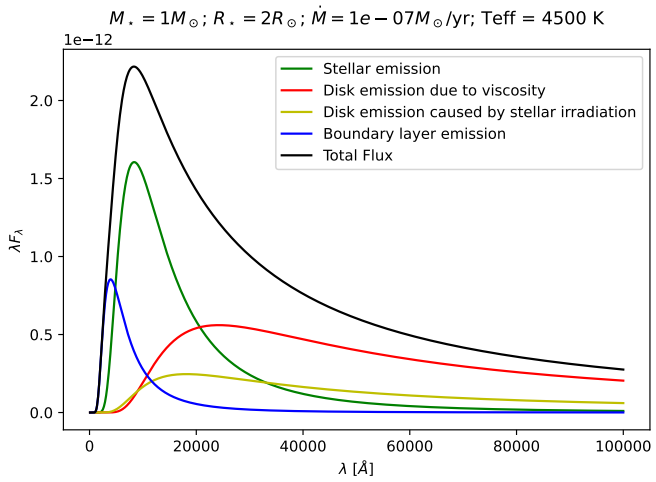

Fig. 9: Total Spectral Emission Distribution (SED), $\lambda F\lambda$, of the system and the emission from each component.

But what if we vary the stellar mass, the mass accretion rate and the effective temperature? Figure 10 shows the total SED for the system in study, while varying these properties. The solid lines represent the original system, while the dotted and dashed lines represent the systems with one determined property varying. The color coding is the same as in figure 9.

The stellar mass $M_\star$ and the mass accretion rate $\dot{M}$ affect only the emission of the disk due to viscosity and the boundary layer, while the effective temperature $T_{\rm eff}$ affect every component except the boundary layer emission. This is to be expected by analysing the derivation of each component's SED. Furthermore, a simple inspection of the shape of the total SED may hint to a specific component being dominant, such as in the case of the middle plot of figure 10, where when $\dot{M} = 10^{-6} M_\odot$/yr there is a visible peak at lower wavelength.

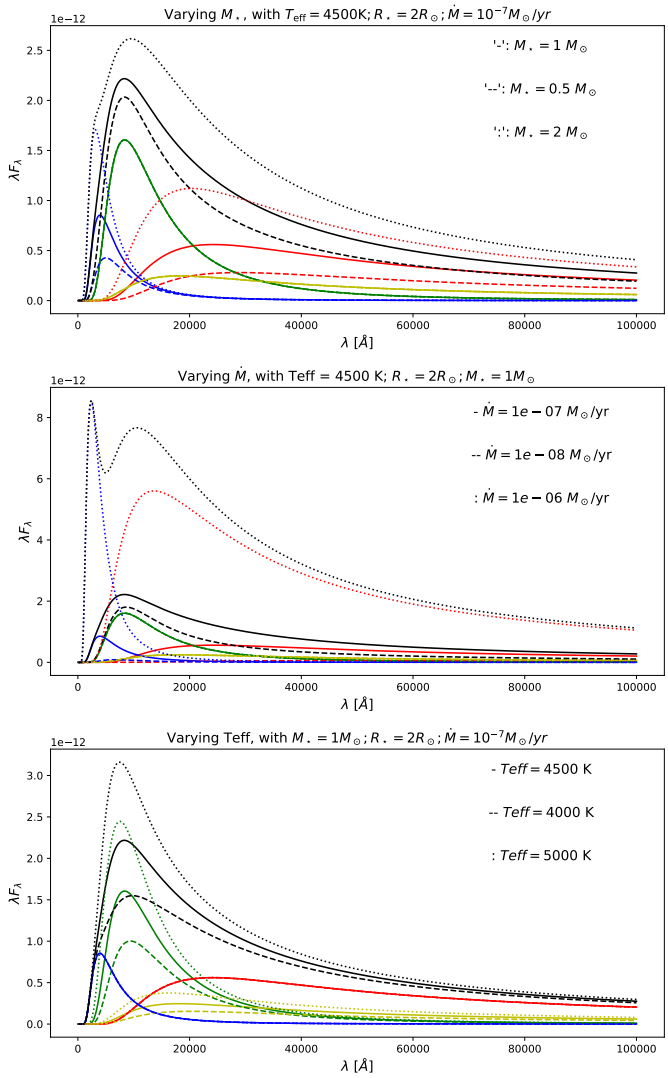

Fig. 10: Total Spectral Emission Distribution (SED) changing the stellar mass, the mass accretion rate and the effective temperature. The color coding is the same as in figure 9. Top: Setting the stellar mass to $1M_\odot$, $0.5M_\odot$ and $2M_\odot$. Middle: Setting the mass accretion rate to $\dot{M} = 10^{-7} M_\odot$/yr, $\dot{M} = 10^{-8} N_\odot$/yr and $\dot{M} = 10^{-6} M_\odot$/yr. Bottom: Setting the effective temperature to $T_{\rm eff} = 4500$ K, $T_{\rm eff} = 4000$ K and $T_{\rm eff} = 5000$ K.

4. Conclusion

In this project, we aimed to unravel the intricate dynamics of viscous accretion disks encircling young stellar systems, spanning analytical and numerical approaches. Through the analytical exploration, we leveraged Lynden-Bell's formulation to unveil fundamental properties of accretion disks, shedding light on mass redistribution phenomena influenced by viscosity variations and boundary conditions. Additionally, our numerical simulations allowed for a detailed examination, unveiling nuanced effects of viscosity variations on disk evolution. We discovered that as viscosity increased, the mass tended to accumulate near the disk's center, exhibiting a distinct bulk motion behavior.

Transitioning from accretion disk dynamics to SED estimation, we delved into the complex interplay of emission components contributing to the overall SED of stellar systems with circumstellar disks. Our analysis considered stellar black-body emission, disk viscosity, stellar irradiation, and boundary layer emission. We uncovered that variations in stellar properties, such as mass, mass accretion rate, and effective temperature, influenced greatly the total SED, shaping emission characteristics across different wavelengths.

Furthermore, the sensitivity of the SED to variations in stellar properties emphasized the importance of considering these parameters in understanding emission characteristics comprehensively.

In conclusion, our work has not only provided a broad understanding of the evolution and emission properties of viscous accretion disks surrounding young stellar systems. By combining analytical and numerical methodologies, we have uncovered valuable insights, contributing to our broader comprehension of star formation and disk evolution.

References

Frank, J., King, A., & Raine, D. 2002, in Accretion Power in Astrophysics, ed. 3, Cambridge Astrophysics, Cambridge University Press
Gameiro, J. F. S. 2024, in Accretion Disks, Physics and Astronomy Department of University of Porto Faculty of Sciences
Lynden-Bell, D., & Pringle, J.E. 1974, MNRAS, 168, 603-637
Langtangen, H. P., & Linge, S. 2017, in Finite Difference Computing with PDEs. A Modern Software Approach, ed. 1, Springer

Appendix A: Extra figures for Section 2

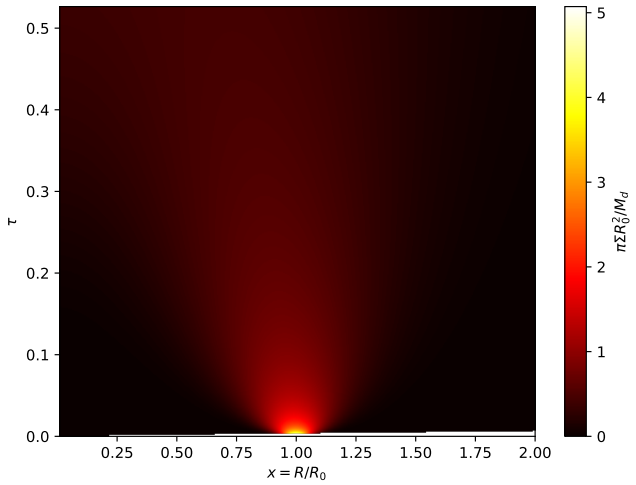

Fig. A.1: Evolution of the surface mass density in normalized time and distance for the analytical method. The white strip in the lowest part of the plot is unexplained.

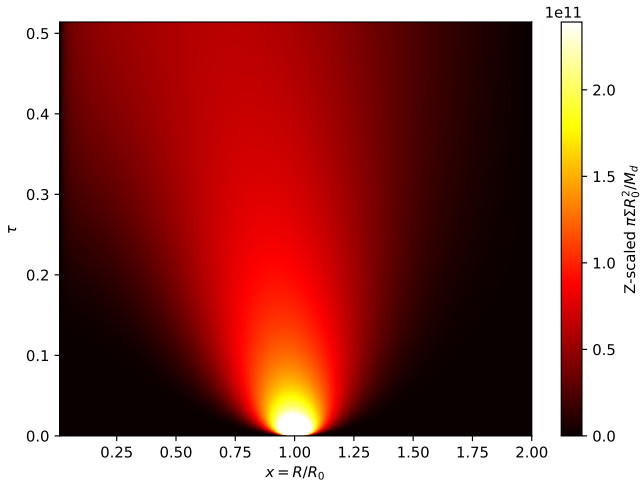

Fig. A.2: Evolution of the surface mass density in normalized time and distance for the numerical method.